I&EC research
Industrial & Engineering Chemistry Research
pubs.acs.org/IECR
Article

Pilot-Scale Optimization of the Solvent Exchange Production and Lyophilization Processing of PEG–PLA Block Copolymer-Encapsulated $CaWO_4$ Radioluminescent Nanoparticles for Theranostic Applications

Anish P. Patel,[†] Christopher R. Schorr,[†] Dhushyanth Viswanath, Kaustabh Sarkar, Natalie J. Streb, Vincenzo J. Pizzuti, Rahul Misra, Jaewon Lee, and You-Yeon Won*

Cite This: *Ind. Eng. Chem. Res.* 2021, 60, 7081–7096

ABSTRACT: Previous studies have shown that calcium tungstate ($CaWO_4$) nanoparticles (NPs) can be used as a radiosensitizing/X-ray contrast agent for cancer treatment. However, due to the propensity of calcium tungstate to agglomerate in physiological solutions, there is a need to encapsulate these NPs within poly(ethylene glycol)-poly(D,L-lactic acid) (PEG–PLA) polymeric micelles through a solvent exchange process. Several parameters including solvent type, polymer to NP ratio, mixing method, and lyophilization were studied to optimize the encapsulation and storage procedures for future scale-up. Herein, we report that the cosolvent that was previously used in this procedure (dimethylformamide) can be replaced with a less toxic cosolvent (acetone), the polymer to NP ratio can be reduced from 600:1 to 50:1 without increasing the particle size by 20%, and mixing methods that create a more uniform flow field produce a more homogenous and less polydisperse particle distribution. In addition, our results indicate that sucrose as a lyophilization excipient produces less agglomeration during freeze-drying compared to mannitol. The smaller molecular weight 2 kDa and 2 kDa ("2 k–2 k") PEG–PLA was less prone to agglomeration during freeze-drying compared to 5 k–5 k PEG–PLA.

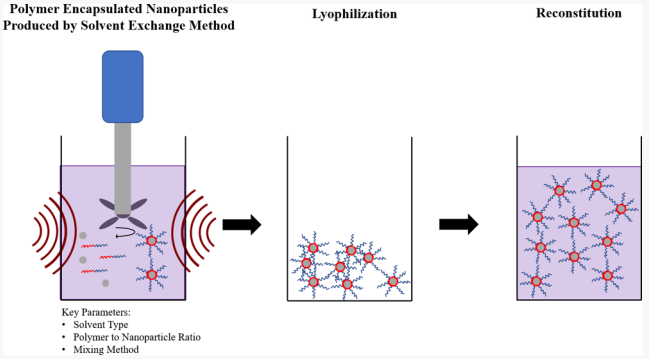

1. INTRODUCTION

Nanomedicine has become a big focus in cancer research because of its potential to overcome the physical and biochemical obstacles that are characteristic of tumor physiology with regards to drug transport.[1,2] Moreover, standard generic therapies that are currently available for treatment of cancer, including chemotherapy and radiation therapy, are associated with toxicities, side effects, and inefficiencies that may be dealt with by using nanoparticulate drug delivery systems.[1−3] The nanometer scale of these systems is believed to provide some advantages over traditional therapies including improved targeted delivery, bioavailability, physiological stability, and reduced toxicity.[4] An important subset of such systems includes nanoparticles (NPs) encapsulated within biodegradable, amphiphilic block copolymer (BCP) assemblies.

BCP assemblies have been found to be an effective method for drug delivery due to their ability to self-assemble into stable nanostructures (such as micelles) in an aqueous environment. Micelles formed through a self-assembly of BCPs have been widely used to increase the effective solubility (and thus bioavailability) of highly hydrophobic drugs.[5] In addition to organic chemotherapeutic drugs, inorganic NP formulations have been developed with the aim to expand the scope of the available cancer treatment options. For example, chemotherapeutic drugs, such as paclitaxel, have been extensively studied in the context of polymeric NP encapsulations.[6] Furthermore, significant research has been conducted to study the potential of inorganic materials such as gold, silver, iron oxide, and calcium tungstate ($CaWO_4$ or CWO for short) NPs in biomedical imaging and treatment applications.[7−11]

Polymeric NPs are typically produced through a solvent exchange (nanoprecipitation) process, in which free polymer and active pharmaceutical ingredients (APIs) are initially dissolved in an organic cosolvent and encapsulated NPs precipitate upon the addition of an antisolvent (water). Drug/NP-loaded polymer NPs have been most commonly produced using batch-type solvent exchange processes. Recently,

Received: November 27, 2020
Revised: April 22, 2021
Accepted: April 28, 2021
Published: May 6, 2021

https://doi.org/10.1021/acs.iecr.0c05852
Ind. Eng. Chem. Res. 2021, 60, 7081–7096

Table 1. Summary of Previous Literature Solvent Exchange Methodology[a]

NP used	solvent used (safety class)	polymer used	encapsulated particle diameter (nm)	initial polymer to NP ratio (by weight or as specified)	mixing method	reference
Au	chloroform(II)	PEG(5.0 k)-PLGA(8.0 k)	60	NR	sonication	19
Au	DCM(II)	PEG[30 wt %]-PLA[70 wt %]	230−260	NR	dispersion (5 min, 2000 rpm)	20
Au	DMF(II)	PEG(7.0 k)-PnBA (7.3 k)	75	NR	sonication (30 min)	18
		PEG(7.0 k)-PnBA(11.4 k)	NR	NR		
$CaWO_4$	DMF(II)	PEG(∼5.0 k)-PnBA(5.8 k)	70	100	dispersion (15,000 rpm) and sonication (30 min)	14
			60			
			40			
		PEG(5.0 k)-PLA(3.3 k)	190			
			175			
			165			
Fe_3O_4	chloroform(II)	PEG(3.5 k)-PLA(240.0 k)	200−400	19	sonication (40 min) followed by magnetic stirring (2000 rpm)	21
				5.67		
				3		
Fe_3O_4	chloroform(II)	PEG(3 k)-PLA(20.4 k) linked with PSA mAb	240 ± 2	1	sonication	22
Fe_3O_4	DCM(II)	mPEG(2.0 k)-PLA(1.3 k)	70−73	2 (assuming constant 0.2 g polymer and 2 mg/mL NP solution)	magnetic stirrings (24 h)	23
		FA-PEG(2.0 k)-PLA(1.3 k)				
		PEG(3.0 k)-PLGA(∼13.4 k)	35 ± 13			
		PEG(4.0 k)-PLGA(∼12.4 k)	29 ± 11			
Fe_3O_4	DCM(II)	scAb-PEG(3.4 k)-PLGA(34.0 k) and mPEG(2.0 k)-PLGA(34.0 K)	187.4 ± 32.7	5	dispersion (5 min) followed by sonication (2 min)	24
Fe_3O_4	DCM(II), THF(II)	FA-PEG(2.0 k)-PLGA(44.0 k)	180	50 or 12.5 (various conditions)	sonication (18 W, 1.5 min) followed by magnetic stirring (overnight)	25
Fe_3O_4	THF(II)	mPEG(5.0 k)-PLA(2.5 k)	85 (including RDG peptide conjugation)	0.15	shaking (overnight)	26
Fe_3O_4	THF(II)	PEG(5.0 k)-PCL(5.0 k)	75 ± 4	5	sonication	27
			97 ± 6	5		
			110 ± 9	5		
ZnPc	DMF(II)	PEG(2.0 k)-PLA(5.0 k)	104 ± 7	19	magnetic stirring (2−3 h)	28
			101 ± 0.5	9		
			117 ± 10	4		
			120 ± 6	4		

[a]NR = not reported. For the polymer used, values in parentheses indicate molecular weight.

https://doi.org/10.1021/acs.iecr.0c05852
Ind. Eng. Chem. Res. 2021, 60, 7081−7096

Table 2. Summary of Previous Literature Lyophilization Excipient Use[a]

active ingredient	polymer encapsulant(s)	lyophilization excipient(s) or lyoprotectant(s)	polymer:lyoprotectant (w/w) ratio range	size increase factor range	reference
N/A	amphiphilic polymeric nanoparticles (example: PEG−PLA)	lactose	1:0.11−1:1.5	NR	29
		maltose			
		sucrose			
		trehalose			
N/A	PCL(14.0 k) (encapsulant), PVA(31.0 k) (stabilizer, 1.25−5% (w/v))	no excipient	N/A	1.39	30
		glucose	1:0.25 or 1:0.5	0.96−1.02	
		sucrose		0.96−1.00	
		HPβCD		1.01−1.05	
		trehalose		0.96−1.00	
		mannitol		1.00	
		maltose		0.99	
		PVP		1.00	
ciprofloxacin HCl	PLGA(40.0 k)	no excipient	NR	1.023−1.025	31
		mannitol	500 mg polymer and 5% w/v lyoprotectant	1.007−1.053	
		trehalose		1.008−1.016	
		glucose		1.015−1.027	
N/A	cationically modified silica nanoparticles	no excipient	NR	∼300	32
		glucose	1:5.6−1:22	∼2−4	
		trehalose		∼1−1.5	
		mannitol		∼2−6	
		sorbitol		∼1.5−2	
		acetic acid		∼7.5−8	
		glycerol		∼1.5−2	
paclitaxel-loaded iron oxide NPs	mPEG(2.0 k)-lysine-di-oleic acid	mannitol	1:0.636−1:3.18	NR (59.1−71.2 nm post-reconstitution)	33
N/A	mPEG(20.0 k)-PLA(45.0 k)	sucrose	1:0.5−1:20	1−4	34
dexamethasone	PEG(5.0 k)-PVP(20.0 k)	sucrose	1:20	2.1	35
		trehalose		1.4	
		SBEβCD		1.0	
		HPβCD		0.7	
		maltose		not redispersible	
		Kolllidon PF17		2.5	
	PEG(5.0 k)-PDLLA(23.0 k)	sucrose		1.0	
		HPβCD		1.0	
	PEG(5.0 k)-PLGA(28.0 k)	sucrose		0.95	
		trehalose		1.2	
		SBEβCD		1.0	
		HPβCD		0.9	
		Kolllidon PF17		1.8	
	PEG(5.0 k)-PCL(32.5 k)	SBEβCD		1.8	
		HPβCD		0.95	
		maltose		1.7	
sagopilone	PEG(2 k)-PLA(2.2 k)	mannitol	1:1	∼1.05	36
		sucrose		∼1.05	
	PEG(2 k)-PCL(2.6 k)	HPβCD	1:20	∼2	
		PVP		∼1.25	
	PEG(5 k)-PCL(5 k)	HPβCD	1:20	∼0.67	
		PVP		∼1.15	
N/A	PEG(2 k)-PLA(2.2 k)	mannitol	1:1	∼1.14	
		sucrose		∼1.1	
	PEG(2 k)-PCL(2.6 k)	HPβCD	1:20	∼5	
		PVP		∼1.3	
	PEG(5 k)-PCL(5 k)	HPβCD	1:20	∼0.77	
		PVP		∼1.1	
N/A	PEG(2 k)-PLA(100 k)	no excipient	NR	1.1	37
		trehalose	1:2	1.0	
	PEG(5 k)-PLA(100 k)	no excipient	NR	1.5	
		trehalose	1:2	1.0	
	PEG(10 k)-PLA(100 k)	no excipient	NR	2.8	
		trehalose	1:2	1.0	

https://doi.org/10.1021/acs.iecr.0c05852
Ind. Eng. Chem. Res. 2021, 60, 7081−7096

Table 2. continued

[a]NR = not reported. For the polymer used, values in parentheses indicate molecular weight

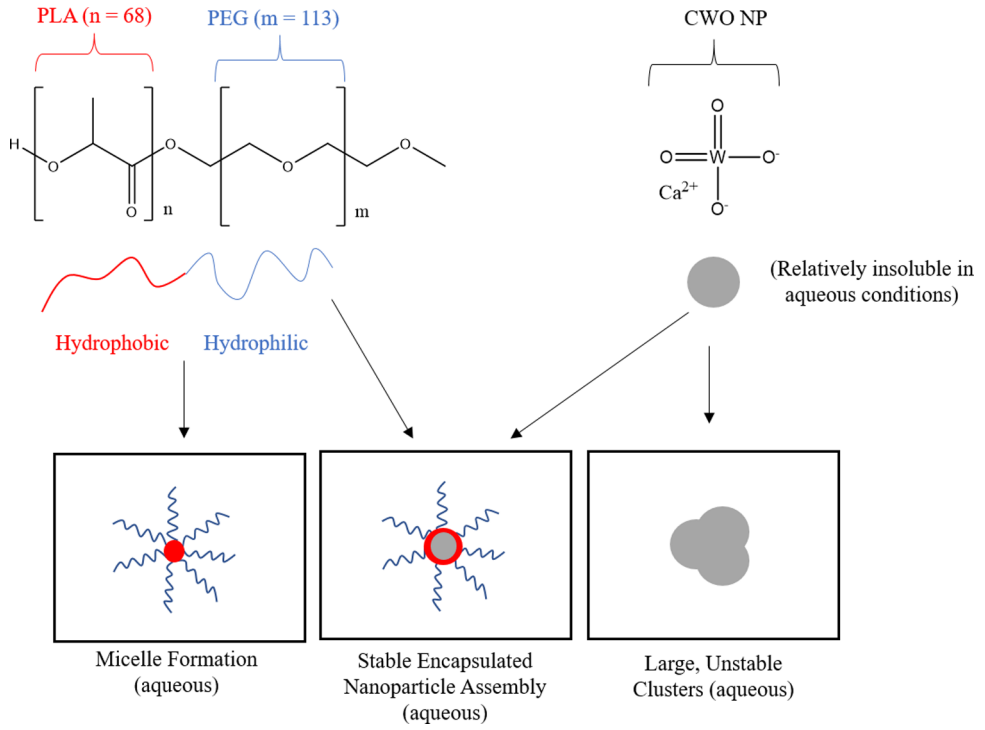

Figure 1. PEG−PLA is an amphiphilic block copolymer with the ability to encapsulate water-insoluble calcium tungstate nanoparticles (CWO NPs) into micelles, allowing CWO NPs to become bioinert.[14]

researchers have also developed continuous solvent exchange processes involving high-efficiency micromixers (termed flash nanoprecipitation).[12] However, the conventional batch solvent exchange method is still the most common method of choice for producing pharmaceutical polymer nanoformulations.

In conventional solvent exchange processes, the key process parameters that control the properties of the polymer-encapsulated NPs produced are solvent type, polymer to NP ratio, and mixing method. Despite the large amount of publications reporting the use of this method, there has been a lack of systematic investigation of these parameters. For instance, potential safety issues have not previously been considered as a factor in the selection of cosolvents for solvent exchange. As summarized in Table 1, the most commonly used cosolvents [e.g., tetrahydrofuran (THF), dimethylformamide (DMF), and dichloromethane (DCM)] are all Safety Class II chemicals,[13] which would require more stringent downstream purification steps. It has not previously been studied whether a safer cosolvent (e.g., acetone, Safety Class III) could be used for solvent exchange with similar results. Also, in most previous studies, excess amounts of polymer have been used without rationalization of the molecular mechanisms taking place (e.g., adsorption kinetics); see Table 1. Without a detailed mechanistic understanding, it becomes difficult to optimize the amount of polymer to be used, and excess polymer imposes further burden on reagent cost and purification. Lastly, several different mixing methods (sonication, magnetic stirring, dispersion, etc., as summarized in Table 1) have been employed in previous studies without a thorough comparison across these methods. Currently, little information is available regarding how mixing affects the size characteristics of encapsulated NPs.

In most basic/preclinical research studies in which NP-loaded polymer micelles were explored (as listed in Table 1), as-prepared formulations were typically used for immediate characterizations. However, for real clinical applications, long-term storage is a critical issue. This is especially relevant to systems in which the API is a small-molecular drug that can spontaneously diffuse out of the carrier system over time. A common approach to address this issue is to lyophilize, or freeze-dry, the formulation. For this reason, lyophilization has been a topic of research interest in this field, as shown in Table 2. To our knowledge, there has been little study into the effects of NP loading on the lyophilization of polymer micelles. Unlike small-molecule drugs, NPs are typically larger than polymers, and for this reason, their presence inside the core of a polymer micelle may affect the conformation of the polymers and thus the stability of the formulation during lyophilization.

In the present study, we attempt to address the aforementioned issues in the formulation of CWO NPs encapsulated within poly(ethylene glycol)-poly(D,L-lactic acid) (PEG−PLA) micelles that can be used for cancer treatment.[11,14−16] CWO has been found to possess unique radioluminescent properties, allowing it to act as a radiosensitizer by increasing a tumor's susceptibility to lower doses of radiation and therefore reducing the probability of side effects associated with radiation therapy. CWO NPs are also promising materials for use as X-ray computed topography (CT) contrast agents.[17] Because CWO NPs tend to agglomerate in aqueous physiological environments, it becomes necessary to encapsulate the NPs within a BCP micelle, such as one that is composed of hydrophilic PEG and hydrophobic PLA. Through an established solvent exchange method, the CWO NPs can be encapsulated into the polymeric

https://doi.org/10.1021/acs.iecr.0c05852
Ind. Eng. Chem. Res. 2021, 60, 7081−7096

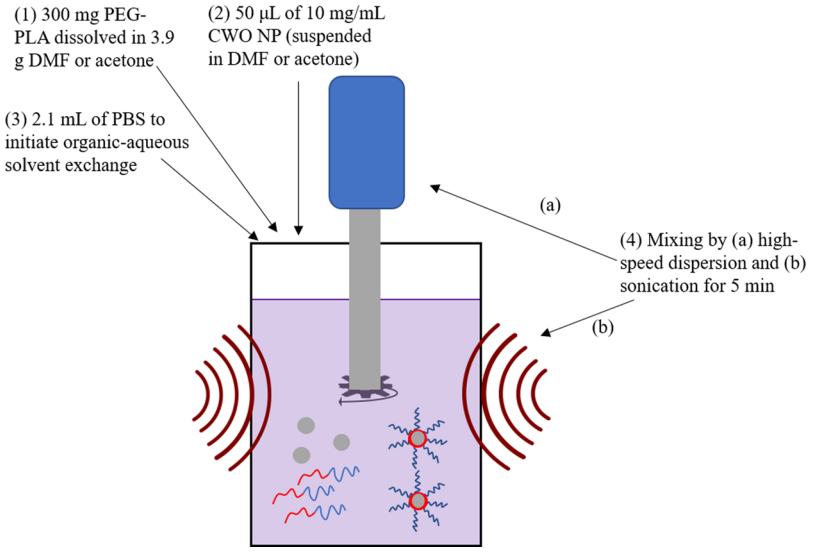

Figure 2. Procedure to encapsulate calcium tungstate nanoparticles (CWO NP) into amphiphilic block copolymer (PEG−PLA) micelles.

micelles, making them suitable for intratumoral administration, as seen in Figure 1.[8,18]

Although the established procedure for CWO NP encapsulation (detailed in the Experimental Methods) is currently being utilized for various in vivo studies, it can likely be improved to be more consistent with pharmaceutical recommendations. Several parameters were investigated in order to reduce the toxicity and the costs of the reagents used including solvent type, mixing method, polymer to NP ratio, and lyophilization. These factors were studied in order to explore their effects on the final NP-encapsulated polymer micelle size characteristics including hydrodynamic diameter and polydispersity index (PDI). To address the issue of solvent toxicity, our laboratory group investigated the use of acetone (Class III) as an alternative to the previously used cosolvent, DMF (Class II). Next, the effect of the polymer to NP ratio was studied to determine whether the amount of the polymer could be reduced without significant size alteration. Four different mixing methods (sonication, dispersion, sonication/dispersion, and stirring) were employed to measure the influence of mixing on the system. Lastly, a lyophilization step was added to the procedure to determine its effects on particle size after reconstitution. Two common lyophilization excipients (sucrose and mannitol) were used at two different concentrations and assessed along with reconstitution time and PEG−PLA molecular weight.

2. EXPERIMENTAL METHODS

2.1. Synthesis and Evaluation of PEG−PLA and CWO NPs. The PEG−PLA BCPs were synthesized via ring-opening polymerization of racemic lactide with PEG precursors, as previously described.[14] For PEG−PLA, 0.45 g of monomethoxy monohydroxy PEG (CH_3O-PEG-OH, Sigma, M_n = 5.0 or 2.0 kDa) and 0.45 g of racemic lactide were added to a round bottom flask, and the flask was heated to 70 °C, evacuated under vacuum for 30 min, and purged with argon gas, and then, 22 mL of anhydrous DCM (Sigma) was added to dissolve the reactants. The reaction was catalyzed by 1,8-diazobicyclo[5.4.0]unde-7-ene (DBU, 98%, Sigma), with 0.22 mmol dissolved in 2 mL of DCM added directly to the reaction vessel. The reaction was run for 2 h at room temperature and was terminated by adding 15 mg of benzoic acid (>99.5%, Sigma). PEG−PLA was precipitated by the dropwise addition of the reaction solution to 1 L of mixed hexanes (Thermo Fisher). The precipitate was then dried overnight in a vacuum oven. The molecular weights (M_n's) of the PLA blocks were determined to be 4.8 ± 0.1 kDa for 5 k−5 k PEG−PLA and 1.9 ± 0.1 kDa for 2 k−2 k PEG−PLA by ^{1}H NMR spectroscopy. The overall molecular weight polydispersity indices were about 1.1 for both of the polymers [determined by gel permeation chromatography (GPC) with THF as the mobile phase].

All results reported in Sections 3.1−3.3 were obtained using 5 k−5 k PEG−PLA. Both 5 k−5 k PEG−PLA and 2 k−2 k PEG−PLA were used in the study discussed in Section 3.4.

CWO NPs were synthesized via a microemulsion method as previously described, with some modification.[11,14] Briefly, 10.0 mL of cyclohexane was mixed with 1.0 mL of 1-hexanol (Sigma) and 1.0 mmol of CTAB (Sigma) and subsequently stirred at 70 °C until it was transparent. Then, two separate solutions were made: one with 0.20 mmol of Na_2WO_4 dissolved in 0.30 mL of Milli-Q-purified water and one with 0.20 mmol of $CaCl_2$ in 0.282 mL of Milli-Q water and 0.018 mL of 0.10 M HCl. These aqueous solutions were then immediately added to the first solution and vigorously stirred for 1 min. The solution was then transferred to a Teflon-lined stainless-steel autoclave and baked in an oven at 160 °C for 24 h. Afterward, the autoclave was gradually cooled, and the NPs were separated and purified via centrifugation and ethanol/chloroform washes (repeated at least 3 times). The final solid was dried overnight in a vacuum oven at room temperature. The mean diameter of CWO NPs was measured to be approximately 33 nm by transmission electron microscopy (TEM).[8,14]

2.2. Standard Preparation of BCP-Encapsulated CWO NPs by the Solvent Exchange Process. The procedure used for the encapsulation of CWO NPs with the PEG−PLA (5 k−5 k) BCP has been adapted from previously used methods[14] and is outlined in Figure 2. A 300 mg sample of the PEG−PLA polymer was dissolved in 3.9 g of DMF (99.8%, Sigma). A 50.0 μL aliquot of 10 mg/mL CWO NPs (suspended in DMF and ultrasonicated for 20 min) was then added to the polymer solution. Mixing was introduced to the system using ultrasonication, which served to mildly agitate the species present in the system with sound waves, and a high-speed mechanical disperser machine, which applied 5000 rpm rotation to the

https://doi.org/10.1021/acs.iecr.0c05852
Ind. Eng. Chem. Res. 2021, 60, 7081−7096

system. Immediately afterward, 2.1 mL of phosphate buffered saline (PBS, Ambion, Buffer pH 7.4) was added in order to begin an organic aqueous solvent exchange process. The mixture was left to be sonicated with simultaneous dispersion for 5 min. Following that, the mixture was centrifuged for 10 min at 5000 rpm [equivalent to 3214 × g, Eppendorf 5804 (F-34-6-38, radius of rotor = 11.5 cm)]. The resulting pellet was resuspended in 2.0 mL of PBS. A 0.10 mL aliquot of this suspension was diluted by a factor of 10 and characterized for size as the prefiltration sample. The rest of the suspension was passed through a 0.2 μm PVDF filter and then characterized as the postfiltration sample.

2.3. Characterization of Uncoated and Coated CWO NPs. Filtration effects on uncoated CWO NPs were measured and studied in detail. To do so, a CWO NP stock solution with a concentration of 10 mg/mL in DMF was first agitated using an ultrasonication bath for 20 min, and 50.0 μL was diluted to a final CWO NP concentration of 0.1 mg/mL. The diluted CWO NP sample was then either filtered (using a 0.45 μm PTFE filter) or left unfiltered for size and polydispersity measurement using a Brookhaven ZetaPALS machine and for TEM microscopy using a Tecnai T20 microscope. TEM micrographs of both unfiltered and filtered CWO NPs were obtained by drying 3 μL of each sample on a 50-mesh TEM grid. Both filtered and unfiltered sample calcium concentrations were measured by atomic absorption spectroscopy (AAS) in order to determine the filtration yield which is defined as the ratio of postfiltration CWO mass relative to prefiltration CWO mass. Samples were prepared for AAS by digesting 50 μL of each sample with 50 μL of inhibitor-free sulfuric acid followed by dilution to 5 mL with Milli-Q water. Our group performed AAS using a Perkin Elmer PINAACLE900 Atomic Absorption spectrometer. Lastly, X-ray diffraction (XRD) pattern of unfiltered uncoated CWO NPs was carried out by suspending CWO NPs in chloroform (1 mg/mL), drying the sample on a glass slide to form a thin film, and performing measurement on a flat stage using a Rigaku Smartlab XRD operated on Bragg Brentano mode.

The encapsulation efficiency of the PEG−PLA BCP encapsulation of CWO NPs was also determined using flame AAS. PEG−PLA-encapsulated CWO NPs were prepared using the standard procedure described in the previous section, with mixing of 13,000 rpm dispersion speed for 3 min, and filtration through a 0.45 μm PTFE filter. One hundred microliters of the PEG−PLA/CWO NP sample in PBS was dissolved in 100 μL of trace metal-free sulfuric acid by vortex mixing and letting it rest for 15 min. The sample was then topped up to 5 mL with Milli-Q water and mixed thoroughly before analyzing the calcium content using flame AAS. Calcium standards from 0.1 to 1 ppm were used to generate a calibration curve. The mass of CWO remaining in the samples after filtration with a 0.45 μm PTFE filter was compared to the known initial calcium amount to calculate the encapsulation efficiency.

Lastly, weight loss profiles of unfiltered and filtered PEG−PLA/CWO NPs were obtained using thermogravimetric analysis (TGA) (Q600 SDT, TA Instruments) in order to calculate the PLA layer thickness, PEG grafting density, and loading efficiency, which is defined as the ratio of CWO mass relative to total mass of the polymer-coated NPs. PEG−PLA/CWO NPs in PBS were centrifuged and dried overnight in a vacuum oven to obtain a solid pellet. The pellet was scraped from the vial and added to an alumina crucible. The sample was heated under a helium environment from room temperature to 700 °C at a heating rate of 10 °C/min and held there for 15 min. Initial weights of unfiltered and filtered samples were 3.9 and 0.3 mg, respectively.

2.4. Optimization and Modification of Standard Preparation: Solvent Type, Polymer:NP Ratio, and Mixing Method. For all subsequent experiments, the standard protocol described in Experimental Methods, Subsection 2.2, was used as the starting point. The solvent type was the first parameter investigated in the solvent exchange process. DMF, the organic solvent previously used, was compared to acetone, a safer solvent. Effective diameters of the encapsulated NPs were compared among batches encapsulated with the DMF−PBS solvent exchange and the acetone−PBS solvent exchange procedures (mass ratio of 65% acetone to 35% PBS). A molecular comparison of DMF and acetone is given in Figure 3.

	N,N-dimethylformamide (DMF)	Acetone
	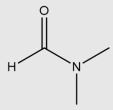	
Safety (Q3C Guidelines)	Class II Solvent (undesired)	Class III Solvent (safer alternative)
Boiling Point	152.8°C (very high)	56.1°C (very low; highly volatile – desirable for separation)
Dielectric Constant (ε)	38.3 (relatively more polar)	21.0 (relatively less polar)
Miscible in H_2O?	Yes	Yes

Figure 3. Comparison of two organic solvents being studied: DMF (the solvent to be replaced) and acetone (a potentially viable replacement).[13,38]

The next parameter that was studied was the polymer-to-NP weight ratio ("Pol:NP"). The standard protocol utilized 300 mg of the PEG−PLA polymer to encapsulate 0.50 mg of CWO NP (600:1). The ratio was varied by first dissolving 600 mg of PEG−PLA in 7.8 g acetone and then aliquoting and diluting as necessary to achieve 3.9 g of PEG−PLA dissolved in acetone with 300:1, 200:1, and 10:1 Pol:NP ratios by weight. The solvent exchange procedure was then carried out as before by adding 2.1 mL of PBS under mixing by sonication and dispersion.

The mixing method used during solvent exchange was assessed next. The previous method utilized combined ultrasonication and high-speed dispersion. The methods evaluated in this study included combined sonication (8892, Cole-Parmer) and dispersion (T25 digital ULTRA TURRAX, IKA), sonication only, dispersion only, and neither sonication nor dispersion [and instead, a simple magnetic stir bar (10 mm length, Teflon coated)]. All samples used DMF and were mixed for 5 min immediately after adding 2.1 mL of PBS. The magnetic stir bar speed was set to 350 rpm. A summary/comparison of mixing methods is shown in Figure 4.

2.5. Lyophilization. An extensive study was conducted to permit and optimize the addition of a lyophilization step. A few key parameters associated with the freeze-drying process were assessed: the excipient type (sucrose or mannitol), excipient concentration (0, 10, or 60% by total dry starting weight, defined as the weight of excipient divided by the weight of PEG−PLA plus excipient), reconstitution time (1, 5, or 30 min), and molecular weight of PEG−PLA (5 k−5 k or 2 k−2 k). The

https://doi.org/10.1021/acs.iecr.0c05852
Ind. Eng. Chem. Res. 2021, 60, 7081−7096

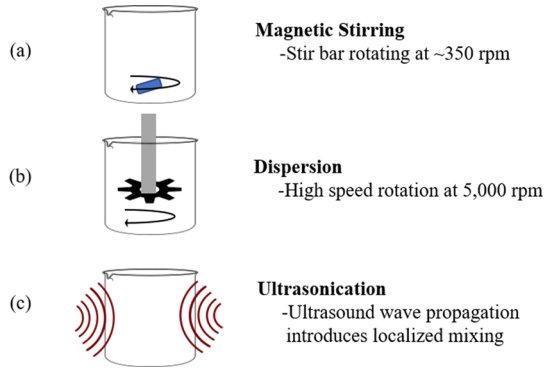

Figure 4. Summary of three mixing methods that were studied to replace original simultaneous sonication/dispersion method: (a) magnetic stir bar, (b) dispersion only, (c) ultrasonication only.

excipient study used 5 k−5 k PEG−PLA and long enough time to ensure complete reconstitution. The reconstitution time study used 5 k−5 k PEG−PLA and 60% sucrose as the excipient. The molecular weight study used 60% sucrose as the excipient and 5 min reconstitution time.

The procedure that was used for the lyophilization experiments followed the original procedure closely, except that the following changes were introduced. Acetone was used as the organic solvent to dissolve the polymer. The postcentrifugation pellet was resuspended in 3.0 mL of PBS to provide enough volume for the added lyophilization step. The excipient was added right before the filtration step at a given concentration as defined above. Complete dissolution was achieved by using a vortex mixer as necessary. One-third of the resuspended volume (1.0 mL) was transferred to a Falcon tube as the prefiltration sample to be lyophilized. Next, because the pellet was resuspended in 3.0 mL instead of 2.0 mL, the dilution factor for the prefiltration samples was 6.67× dilution instead of 10× to maintain the original concentration. As a result, a 0.15 mL aliquot of the remaining 2.0 mL was diluted (6.67×) to 1.0 mL and characterized as the prelyophilization/prefiltration sample. The remaining 1.85 mL was passed through a 0.2 μm PVDF filter, tested as the prelyophilization/postfiltration sample, and then transferred to another Falcon tube as the postfiltration sample to be lyophilized. Both Falcon tubes, each containing 1.0 mL of the sample, were placed in a freezer at −80 °C for 30 min and then transferred to a lyophilizer chamber and dried overnight, while being thawed in the lyophilization machine (FreeZone 4.5 Plus, Labconco) at a collector temperature of −86 °C in a vacuum (pressure of approximately 0.027 mbar). Freeze-dried products were reconstituted in 1.0 mL of PBS, applying vortex mixing as necessary, for a given amount of reconstitution time. The postlyophilization/prefiltration sample (diluted by 6.67×) and postlyophilization/postfiltration sample were then characterized for size and size distribution by dynamic light scattering (DLS). The size increase factor was calculated as the postlyophilization diameter divided by the prelyophilization diameter.

2.6. Size Characterization Using DLS. The main parameter of interest in these optimization experiments was the final encapsulated NP product size. All size characterizations were made on aqueous samples using the DLS technique (ZetaPALS, Brookhaven Instruments) at a scattering angle of 90°. Due to inevitable loss of NPs in multiple steps of the procedure, especially when passed through the filter, the approximate concentration of CWO NPs of the samples tested in the DLS machine is estimated to be between 0.02 mg/mL (for prefiltration samples that have been diluted by 10× or 6.67× in the lyophilization study, considering typical 20% loss of NPs

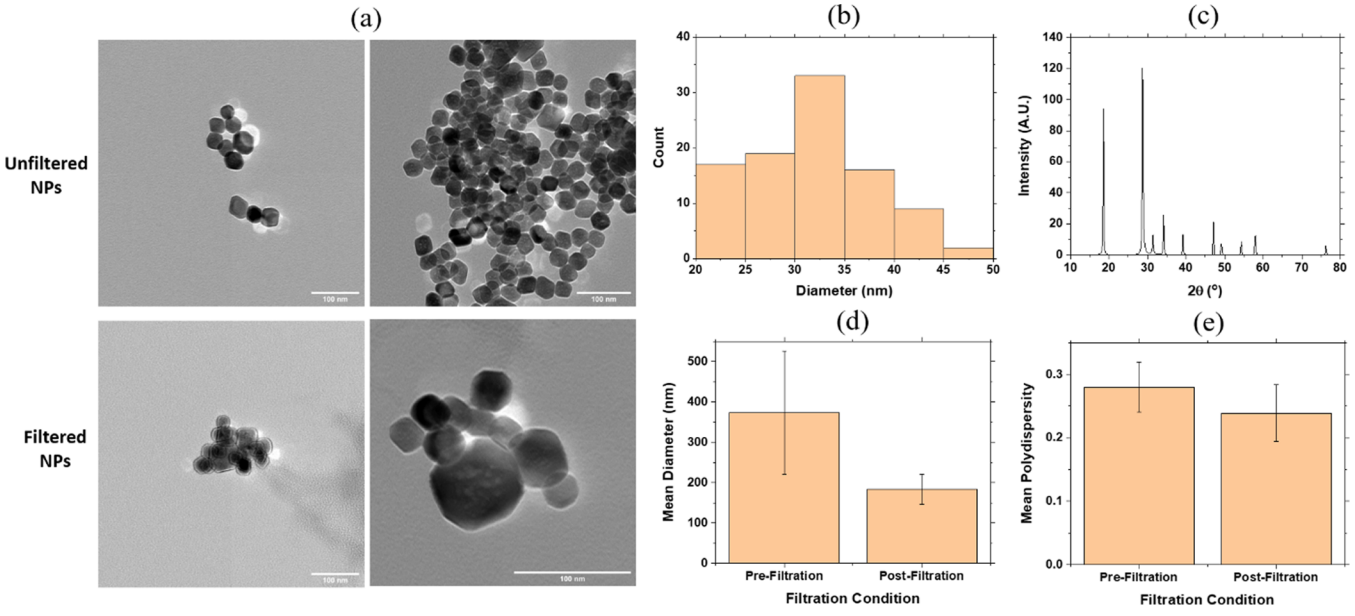

Figure 5. (a) TEM micrographs for uncoated CWO NPs before and after filtration with a 0.45 μm PTFE filter. A total of 3 μL of the sample was dried on a 50-mesh TEM grid and imaged using a Tecnai T20 microscope. (b) Lognormal size distribution for uncoated primary CWO NPs as obtained from TEM micrographs (N = 100). The average size of uncoated primary NPs was 32.7 ± 7.3 nm. (c) XRD pattern of uncoated CWO NPs. The sample was dried on a glass slide to form a thin film and analyzed using a Rigaku Smartlab XRD operated on Bragg Brentano mode. The full width at half maximum (FWHM) for the peak at $2\theta = 28.7°$ is estimated to be 0.234°. Assuming a shape factor of 0.9, the average crystallite size was estimated to be 38.7 nm using the Scherrer equation. (d,e) DLS readings on mean hydrodynamic diameter and PDI of uncoated CWO NPs before and after filtration with a 0.45 μm PTFE filter. Error bars equal ±1 SD representing batch-to-batch variability. N = 3.

https://doi.org/10.1021/acs.iecr.0c05852
Ind. Eng. Chem. Res. 2021, 60, 7081−7096

Table 3. Filtration, Encapsulation, and Loading Characterizations of Uncoated and PEG(5 k)-PLA(5 k)-Coated CWO NPs[a]

	prefiltration	postfiltration
uncoated CWO NP filtration yield (%) (AAS)	N/A	9.2 ± 2.2
CWO encapsulation efficiency (%) for PEG−PLA/CWO NPs (AAS)	N/A	20.9 ± 3.2[b]
composition of PEG−PLA/CWO NPs (volatile:PLA:PEG:CWO by weight) (TGA)	5.2:14.5:12.4:68.0	5.5:6.0:6.1:82.4
CWO loading efficiency (%) for PEG−PLA/CWO NPs (TGA)	71.7	87.2
PLA layer thickness (nm) of PEG−PLA/CWO NPs (TGA)	N/A	1.7
PEG grafting density of PEG−PLA/CWO NPs (# chains/nm^2 CWO surface) (TGA)	N/A	3.5

[a]Uncoated NP filtration yield (from AAS of uncoated CWO NP samples) is defined as mass of calcium after filtration (0.45 μm PTFE) relative to initial mass. Encapsulation efficiency (from AAS of polymer-coated CWO NP samples) is defined as mass of calcium after filtration relative to initial mass. Loading efficiency (from TGA of polymer-coated CWO NP samples) is defined as mass of CWO divided by total polymer + NP mass. PLA layer thickness and PEG grafting density were determined from TGA. [b]Consistent with a value of ∼15% obtained previously using a 20 μm PVDF filter (unpublished).

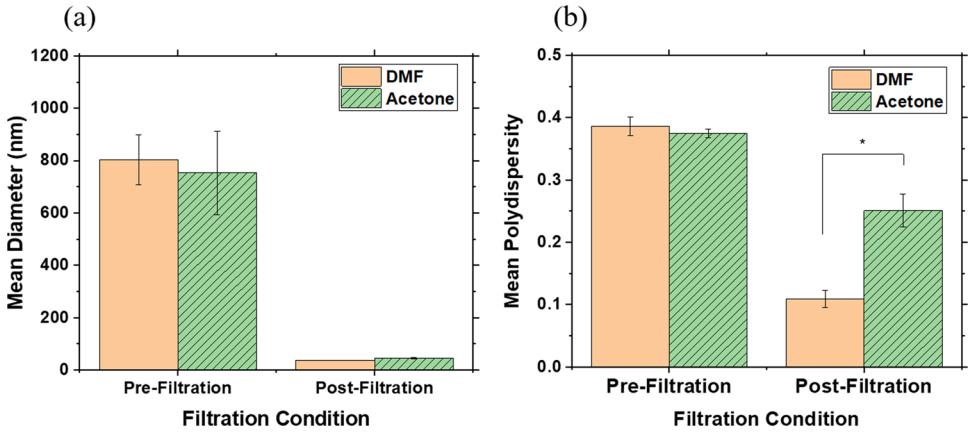

Figure 6. DLS readings on (a) mean hydrodynamic diameter and (b) mean polydispersity index of PEG(5 k)-PLA(5 k) encapsulated CWO NPs based on organic solvent used (DMF vs acetone) before and after passing the sample through a 0.2 μm PVDF filter. Error bars equal ±1 SD, representing batch-to-batch variability. N = 3 for both solvents.

based on prior experience) and 0.03 mg/mL [for postfiltration samples, assuming approximately 85% loss in the filtration step alone (for a 0.2 μm PVDF filter), based on prior experience]. This technique allowed for the measurement of mean hydrodynamic diameter and PDI of the BCP-encapsulated CWO NPs.

2.7. Statistical Analysis. All measurements were in minimum triplicates. In comparing two groups, a t-test was used to determine significant differences. In comparing more than two groups, analysis of variance was used to determine overall statistical significance followed by a post-hoc Games-Howell comparison to evaluate differences between pair combinations. Differences were considered statistically significant (*) if $p < 0.05$ and highly significant (**) if $p < 0.001$. Results are presented in Tables S3−S17 in the Supporting Information section.

3. RESULTS AND DISCUSSION

3.1. Investigation of Uncoated and PEG−PLA-Coated CWO NPs Characteristics. Characterization of the CWO NPs prior to their encapsulation into a BCP assembly was necessary for thorough mechanistic understanding of the encapsulation process. First, we determined the average size of individual uncoated CWO particles via two methodologies: 32.7 ± 7.3 nm via TEM (Figure 5a,b) and 38.7 nm via XRD (Figure 5c). Before filtration, CWO NP agglomeration is present as evidenced by the prefiltration size of the uncoated NPs (Figure 5d) even after 20 min of ultrasonication. During the filtration process, there is a clear reduction in the mean particle diameter of uncoated CWO NPs suspended in DMF (Figure 5e), which suggests that before encapsulation, the uncoated CWO NPs are not completely broken up into individually isolated, pristine particles, but rather, the mixture consists of a heterogenous population of both small and large particles. For our purposes of practical scale-up, 20 min of ultrasonication was sufficient to break apart enough large agglomerates into smaller CWO NPs for PEG−PLA BCP encapsulation. Although these findings may not represent the exact system immediately prior to the encapsulation step, it provides a decent qualitative description of preencapsulated CWO NP population.

Various key parameters pertinent to our study of coated and uncoated CWO NPs are summarized in Table 3. The uncoated NP filtration yield was determined to be 9.2%, and encapsulation efficiency of approximately 20% suggests that filtration does remove the larger-sized populations. Hence, when analyzing our results, we find that unfiltered samples do not provide much useful information to our practical purposes and they should not be expected to follow the same trends as the filtered samples. For the corresponding histograms and TGA, see Supporting Information Figures S1 and S2.

Data summarized in Figure 5 and Table 3 demonstrate that a large number of CWO NPs exist in the form of agglomerates prior to encapsulation (evidenced through characterizations of pre- and postfiltered CWO NPs without encapsulation). Even after 20 min of high-frequency ultrasonication, agglomerates of CWO NPs are still present prior to PEG−PLA encapsulation. These large agglomerates appear to be nondiffusive and thus do not undergo further agglomeration because of their sizes. Only

https://doi.org/10.1021/acs.iecr.0c05852
Ind. Eng. Chem. Res. 2021, 60, 7081−7096

the subpopulation of small-sized (i.e., individual) CWO NPs are effectively encapsulated by PEG−PLA and collected after filtration. For the present study, the preencapsulation process was not optimized; further work is necessary to optimize the break-up of CWO NP agglomerates to yield better encapsulation efficiencies after filtration. However, as will be demonstrated in the following sections, by analyzing filtered samples after encapsulation, we could still accurately investigate the behavior and trends of the smaller encapsulated CWO NPs; the existence of large agglomerates prior to encapsulation does not significantly affect the findings made with filtered particles.

3.2. Solvent Exchange Parameters: Solvent Type and Polymer/NP Ratio. We studied the effect of solvent type on the size characteristics of particles produced by solvent exchange. Specifically, we tested whether acetone could yield similar results to one of the most commonly used solvents, DMF (as discussed in Table 1). The mean hydrodynamic diameter and PDI were measured for each pre- and postfiltered sample prepared using either DMF or acetone. The results are presented in Figure 6. As shown in the figure, the mean diameter of the encapsulated NPs did not change appreciably for both pre- and postfiltered DMF and acetone samples. However, the PDI of acetone postfiltered samples (PDI = 0.25) was significantly higher than that of DMF postfiltered samples (PDI = 0.10); acetone produced a more polydisperse population of NPs on the smaller side.

There are three factors that could have contributed to the observed difference in PDI between acetone and DMF postfiltered samples: the tendency of PEG−PLA to form micelles, the tendency of CWO NPs to aggregate, and the flow introduced by mixing. To characterize the first factor, we performed a simple hydration experiment in which the size of PEG−PLA micelles produced was measured as a function of solvent composition in DMF/water or acetone/water mixtures (Figure S3 of the Supporting Information). As shown in Figure S3, at an identical solvent composition (e.g., at 50% water by volume), PEG−PLA formed smaller micelles in the acetone/water mixture than the DMF/water mixture. This is consistent with the fact that acetone is less polar than DMF; the polarity of the solvent determines the interfacial tension between the solvent and the core PLA domain, which in turn determines the aggregation number (size) for micelles (the less polar the solvent, the smaller is the interfacial tension and thus the smaller the micelles become).[39] A lower interfacial tension between the solvent and core PLA domain would also suggest a lower tendency and slower rate for polymer micellization. This suggests that during the solvent exchange NP encapsulation process, PEG−PLA adsorption to the CWO NP surface occurs at a slower rate in the acetone/water mixture compared to the DMF/water mixture at an identical water percent composition.

The second factor that might have influenced the size characteristics of the particles produced by solvent exchange is the tendency of CWO NPs to aggregate, which may be characterized by the solvent polarity and the resulting van der Waals attractive forces between CWO NPs. As a more polar and denser solvent, DMF has a higher dielectric constant of $\varepsilon_2 = 38.3$ (at 20 °C)[38] and a higher refractive index of $n_2 = 1.43$ (at 20 °C) compared to acetone $\varepsilon_2 = 21.0$ (at 20 °C)[38] and $n_2 = 1.36$ (at 20 °C). Water has a dielectric constant of $\varepsilon_2 = 78.5$ (at 20 °C)[38] and a refractive index of $n_2 = 1.33$ (at 20 °C). $CaWO_4$ has a dielectric constant of $\varepsilon_1 = 10.9$ (at 1.59×10^3 Hz and 25 °C)[40] and a refractive index of $n_1 = 5.25$. Based on this information, the Hamaker constants (A_{121}) for a pair of $CaWO_4$ materials immersed, for instance, in a 50/50 wt % acetone/water mixture ($\varepsilon_2 = 40.6$ and $n_2 = 1.34$) or 50/50 wt % DMF/water mixture ($\varepsilon_2 = 54.8$ and $n_2 = 1.38$) are estimated to be $A_{121} = 1.10 \times 10^{-18}$ J and $A_{121} = 1.09 \times 10^{-18}$ J, respectively; $A_{121} = (3/4)\, k_B T[(\varepsilon_1-\varepsilon_2)/(\varepsilon_1 + \varepsilon_2)]^2 + 3h\nu_e(n_1^2 - n_2^2)^2/[22.6(n_1^2 + n_2^2)^{1.5}]$, where k_B is Boltzmann's constant ($= 1.381 \times 10^{-23}$ J/K), T is the temperature (set to be 293.25 K), h is Planck's constant ($= 6.626 \times 10^{-34}$ J·s), and ν_e is the main electronic absorption frequency in the UV (typically around 3×10^{15} s^{-1}).[41] This calculation suggests that the van der Waals attractive forces between CWO NPs are comparable between the DMF/water and acetone/water mixtures; therefore, the observed difference in PDI between acetone and DMF postfiltered samples cannot be explained by this mechanism.

Lastly, we would like to point out that acetone has different physicochemical properties [η (viscosity) = 0.306 cP at 25 °C, ρ (density) = 0.7902 g/cm^3 at 20 °C)[38] than DMF (η = 0.794 cP at 25 °C, ρ = 0.9445 g/cm^3 at 25 °C),[38] which would produce different mixing effects. For example, at an identical flow velocity (mixing speed), the Reynolds number will be higher with acetone than DMF (by a factor of about 2.2), suggesting more turbulent flow in acetone.

As discussed in detail later in this section, the slower PEG−PLA adsorption in acetone would increase the size of the PEG−PLA-encapsulated CWO NPs. Interestingly, however, this factor did not produce a difference in the mean size of the encapsulated particles. Therefore, we suspect that the effect of the difference in PEG−PLA adsorption speed between acetone/water and DMF/water mixtures on particle size is nullified by a difference in the efficiency of the mixing (i.e., the velocity gradient in the system), which is controlled by the viscosity of the ambient liquid (and thus the Reynolds number of the flow). This argument is based on the following reasoning. First, it should be noted that the mixing method we used for this experimentation (sonication with dispersion as detailed in the Experimental Methods section) establishes a turbulent flow environment; the dispersion alone would produce a Reynolds number of 9690 and 13,899 in DMF and in acetone, respectively (discussed later in this section). In their pioneering study, Camp and Stein proposed that for a general turbulent fluid motion generated by a horizontal impeller in a flocculation tank, the mean velocity gradient (G) is inversely related to the square root of viscosity (i.e., $G = (\phi/\eta)^{1/2}$, where ϕ is the power input per unit volume);[42] to be more precise, it is expected (from the published correlations between the Reynolds number and power number[43]) that $G \sim (\rho/\eta)^{1/2}$ at Reynolds numbers greater than about 10,[3] but note that the difference in density is much less than the difference in viscosity between acetone and DMF (see also the discussion in the next "Mixing Method" subsection). The less viscous mixing environment [and the resulting greater shear field (velocity gradient)] in the acetone system would likely suppress growth of large NP aggregates by fluid mechanically breaking them apart,[44] which thus provides a balance against the effect of the slower PEG−PLA adsorption. Without detailed quantitative analysis, it is difficult to pin down exactly how the combined effects of the slower PEG−PLA adsorption and the greater mechanical suppression of CWO NP agglomeration in acetone were manifested as a higher observed PDI in the filtered NPs (Figure 6), although we suspect that this higher PDI is perhaps due to the accelerating nature of the NP aggregation process (analogous to the nonlinear step growth polymerization[45]). Nevertheless, although there was a slight increase in PDI, which is less favorable from the quality control

https://doi.org/10.1021/acs.iecr.0c05852
Ind. Eng. Chem. Res. 2021, 60, 7081−7096

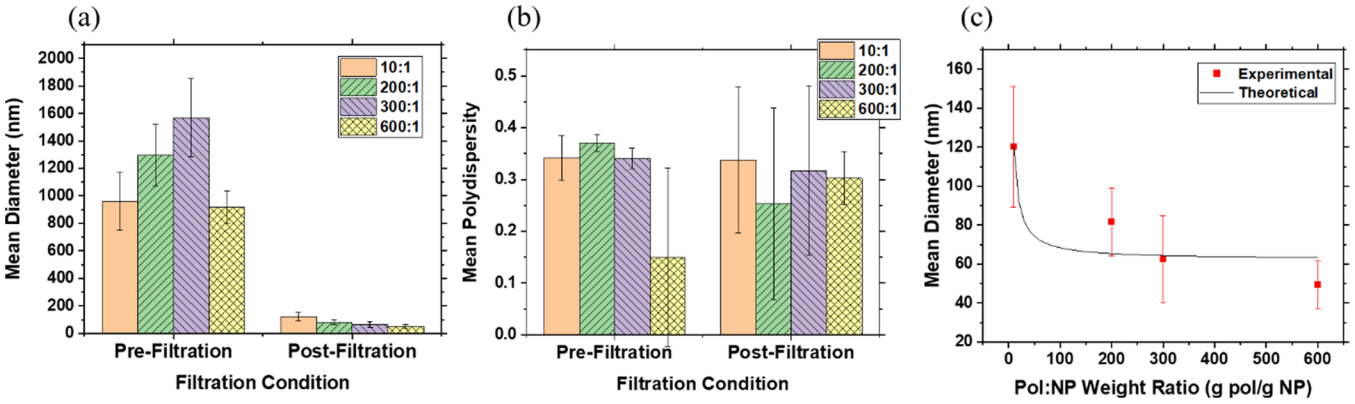

Figure 7. DLS readings on (a) mean hydrodynamic diameter and (b) mean polydispersity index of PEG(5 k)-PLA(5 k)-encapsulated CWO NPs, based on the polymer to nanoparticle weight ratio ("Pol:NP") before and after passing the sample through the 0.2 μm PVDF filter. (c) DLS readings on mean hydrodynamic diameter of postfiltered samples of PEG−PLA-encapsulated CWO NPs as a function of Pol:NP. Discrete data points represent experimental values. The continuous line represents the best fit to the theoretical model described in eqs 1−7. For all graphs, error bars equal ±1 SD representing batch-to-batch variability. N = 3 for all trials.

standpoint, mean particle size does not change appreciably between solvents. Overall, considering acetone's more favorable biosafety profile (Class III) compared to DMF (Class II), acetone was determined to viably replace DMF and is used in some of the subsequent experiments for further investigation.

Next, encapsulated mean particle size was determined as a function of the PEG−PLA amount used relative to the CWO NP amount used in the encapsulation process. The PEG−PLA to NP weight ratio ("Pol:NP") was studied with the objective to reduce the amount of material used to prepare a batch of encapsulated NPs. Under the standard procedure (Pol:NP = 600:1), a majority of polymer molecules are lost as aggregated empty micelles in the centrifugation step. Though there existed variation at each data point, there is a clear negative trend between the Pol:NP ratio and postfiltered mean hydrodynamic diameter (Figure 7).

The marked increase in particle size at lower Pol:NP ratios can be explained by polymer and NP kinetics. Given that the adsorption of polymers and aggregation of CWO NPs are occurring in parallel, the relative rates of each will determine the size of the encapsulated product. The rate of polymer adsorption onto NP surfaces can be modeled by first-order Langmuir kinetics as shown in eq 1,

$$-\frac{\mathrm{d}c}{\mathrm{ct}} = \alpha c\left[1 - \left(\frac{c_0 - c}{c_\theta}\right)\right] \tag{1}$$

where c is the molar (or mass) concentration of the polymer in the bulk solution, c_0 is the initial bulk polymer concentration, c_θ is the polymer concentration required to fully coat the CWO NPs, and α is the adsorption rate constant. The value used for c_θ was based on a Pol:NP ratio of 0.13:0.87 (Table 3) from the TGA profile on CWO NPs encapsulated in PEG−PLA (Figure S2b). Equation 2 shows this differential equation solved with the initial condition that $c(t = 0) = c_0$.

$$\frac{c + c_\theta - c_0}{c} = \frac{c_\theta}{c_0}\exp\left[-\alpha\left(\frac{c_0 - c_\theta}{c_\theta}\right)t\right] \tag{2}$$

The hydrodynamic diameter of the encapsulated NPs can then be modeled by the z-average CWO NP cluster size [$N_z = \frac{\mu_3}{\mu_2}$ where the third and second moments of the cluster size distribution P_i are defined as $\mu_3 = \sum_{i=1}^{\infty} i^3 P_i$ and $\mu_2 = \sum_{i=1}^{\infty} i^2 P_i$, respectively, where $P_i = P_0(1 - p)^2 p^{i-1}$, P_0 is the molar concentration of pristine NPs, p is the conversion of the CWO NP aggregation process ($= (P_0 - P)/P_0$), and P is the total molar concentration of NP clusters ($=\sum_{i=1}^{\infty} P_i$)][45] evaluated at a characteristic time for adsorption of PEG−PLA onto CWO NPs, $t_{0.99}$ [where $c(t = t_{0.99}) = c_0 - 0.99c_\theta$], shown in eqs 3−7,

$$N_z = \frac{1 + 4p + p^2}{(1 - p)^2} \tag{3}$$

$$p = \frac{P_0 \mathrm{kt}}{1 + P_0 \mathrm{kt}} \tag{4}$$

$$k = 8\pi R_0 D_0 N_A \tag{5}$$

$$D_0 = \frac{k_B T}{6\pi\eta R_0} \tag{6}$$

$$R_h \approx R_0 N_z^{1/d_f} \tag{7}$$

where k is the rate constant of CWO NP coagulation at initial stages of the process, R_0 is the pristine NP radius, D_0 is the self-diffusion coefficient of the pristine NPs, N_A is Avogadro's number, k_B is Boltzmann's constant, T is the temperature, η is the solution viscosity, R_h is the mean hydrodynamic radius of CWO NP clusters, and d_f is the fractal dimension of CWO clusters (estimated as 1.8, assuming diffusion-limited colloidal aggregates[46]). Equations 4 and 5 assume rapid (diffusion-limited) irreversible coagulation of CWO NPs,[47] and eq 6 is the Stokes−Einstein equation. Note that for comparison with DLS data, the mean hydrodynamic radius of CWO clusters (R_h) was calculated using the z-average cluster size number (N_z) (eq 7) because DLS determines an average particle size from an intensity-weighted correlation function; in the Rayleigh limit, the scattered light intensity scales with particle (cluster) size to the 6th power ($I \sim R^6$),[48] whereas the particle (cluster) size scales with the number of primary particles within the cluster as $R \sim i^{1/d_f} \sim i^{0.56}$ (eq 7), which gives a scaling relationship between I and i of the type, $I \sim i^{3.3}$; therefore, the z-averaging procedure is a reasonable representation of the intensity-weighted calculation of the mean size. The parameters α and R_0 were adjusted to provide a best-fit model for experimental data, with final values

https://doi.org/10.1021/acs.iecr.0c05852
Ind. Eng. Chem. Res. 2021, 60, 7081−7096

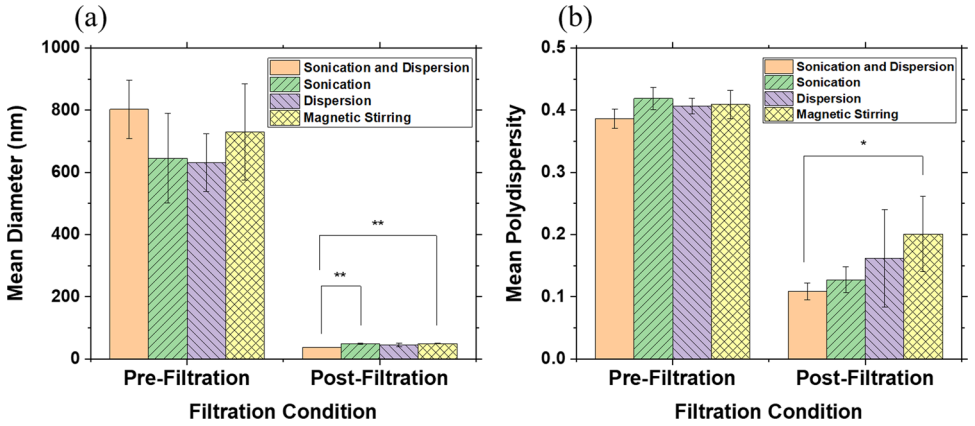

Figure 8. DLS readings on (a) mean hydrodynamic diameter and (b) mean polydispersity index of PEG(5 k)-PLA(5 k)-encapsulated CWO NPs, based on mixing type, before and after passing the sample through a 0.2 μm PVDF filter. Error bars equal ±1 SD representing batch-to-batch variability. From left to right, N = 3, 6, 5, and 6 for each filtration condition.

of $\alpha = 0.235\ s^{-1}$ and $R_0 = 31.2$ nm; these values appear to be very reasonable, particularly when we compare the above-mentioned estimate for R_0 with the value determined by TEM (≈ 32.7 nm). The resulting theoretical model of hydrodynamic diameter versus polymer concentration is compared to the experimental data in Figure 7.

Note that in our theoretical model, we assume that all BCP chains are encapsulating around CWO NPs (no empty micelles). This is a reasonable assumption because CWO NPs serve as heterogeneous nucleation sites for the formation of micelles, and thus, PEG-PLA adsorption to CWO NPs is expected to occur much earlier than the formation of empty micelles via homogeneous micelle nucleation during the solvent exchange process. Also of note, the data reported in Figure 7 are only reported sizes from CWO-loaded micelles, because the centrifugation step used in the sample preparation procedure removes most of the non-loaded micelles (via difference in particle densities).

Expectedly, at a higher polymer concentration and thus a higher adsorption rate, the NPs will be encapsulated before NP clustering becomes significant. As a result, higher polymer concentration would correlate with smaller size. Conversely, at a lower polymer concentration and thus at a lower adsorption rate, the size of encapsulation will be influenced to a larger degree by the rate of NP clustering, in which case the encapsulated NP particle size will be larger. From this analysis, it is clear that the amount of polymer used to prepare encapsulated NPs can be significantly reduced without drastically increasing the size of the product. These results suggest that we can, for instance, reduce the Pol:NP ratio to 50:1 without increasing the size beyond 20% of the original pristine NP size.

3.3. Mixing Method. Mixing during the solvent exchange process can invariably affect the produced size characteristics of the PEG−PLA-encapsulated CWO particles. Encapsulation trials were run using various mixing methods including ultrasonication plus dispersion, ultrasonication alone, dispersion alone, and magnetic stirring to compare particle size characteristics with the previously used method of simultaneous ultrasonication and dispersion; for this experiment, DMF was used as the organic cosolvent. As shown in Figure 8, the mean hydrodynamic diameters of both prefiltered and postfiltered encapsulated NPs were indistinguishable across mixing method groups. Likewise, polydispersity indices varied insignificantly in the prefiltered mixing methods; however, there was a noticeable postfiltration PDI trend across mixing method types. To understand this trend, we investigated whether differences in PDI were due to differences in flow characteristics caused by different mixing methods.

Specifically, we analyzed and compared the power input provided by each mixing method. To estimate the power density of each mixing method, we first calculated the Reynolds number (Re). The Reynolds number is a dimensionless ratio of inertial forces to viscous forces and is a convenient parameter to predict fluid flow turbulence. The Reynolds number for both dispersion and magnetic stirring can be determined using eq 8, where ρ is the density of the fluid, d is the diameter of the impeller, ω is the impeller rotational speed (revolutions per time), and η is the viscosity of the fluid.

$$Re = \frac{\rho d^2 \omega}{\eta} \tag{8}$$

For both dispersion and magnetic stirring, Reynolds numbers were calculated as 1.3×10^4 and 1.4×10,[3] respectively. The turbulent regime is fully developed at Reynolds numbers larger than about 2000 for most small impellers.[49] Therefore, magnetic stirring produces a transition turbulence regime (Re between 20 and 2000), whereas dispersion produces a complete turbulence regime in the acetone/water solution.

Once the Reynolds numbers for both magnetic stirring and dispersion were determined, power usage could be estimated using power number correlations provided by current literature. Power usage was estimated for each mixing type using correlation plots between power number and Reynolds number; based on the impeller geometries, the magnetic stir bar was approximated as a 2-blade paddle and the disperser was approximated as a 20-blade diffuser ring-shrouded turbine stator for the power number versus Reynolds number correlation.[43] In a tank without baffling, the power number for magnetic stirring and dispersion were approximated as 1.00 and 1.05, respectively.

Once the power number of each was found, the power input could be calculated for both magnetic stirring and dispersion using eq 9 given below, where P is the power input, ρ is the fluid density, N_P is the power number, ω is the speed of impeller rotation, and d is the diameter of the impeller.

$$P = \rho N_p \omega^3 d^5 \tag{9}$$

https://doi.org/10.1021/acs.iecr.0c05852
Ind. Eng. Chem. Res. 2021, 60, 7081−7096

Determining the power supplied by ultrasonication required an approach different from the method used for magnetic stirring and dispersion. This is due to a lack of well-defined methods to measure a Reynolds number during ultrasonication. Using the equipment specifications of the laboratory's sonicator, power supply to the sonicator could be calculated using eq 10, where I is the current and V is the voltage supplied to the sonicator.

$$P = IV \tag{10}$$

Once power usage for all three mixing methods was calculated, power density ($\phi = P/V$) could be used to compare the power input per volume across mixing methods used. The volume used for normalization was the volume of fluid the mixing method acted on. For both magnetic stirring and dispersion, the acetone−PBS sample volume was used. For ultrasonication, the ultrasonication bath volume was used.

As shown in Table 4, there is a clear positive trend in power density across magnetic stirring, dispersion, and ultrasonication.

Table 4. Power Density Comparison across Magnetic Stirring, Dispersion, and Ultrasonication

	magnetic stirring	dispersion	ultrasonication
Reynolds number, *Re*	1400	13,900	
power number, N_p	1.00[a]	1.05[b]	
power supplied, P (mW)	4.25×10^{-2}[c]	52.3[c]	3.45×10^{-5}[d]
sample volume, V (mL)	7.04	7.04	5.70×10^{3}[e]
power density, ϕ (mW/L)	6.04	7.42×10^{3}	6.05×10^{4}

[a]Estimated using power number approximation for a two-blade flat paddle. [b]Estimated using power number approximation for a 20-blade diffuser ring-shrouded turbine stator ring. [c]Calculated using eq 9. [d]Calculated using eq 10. [e]Ultrasonication bath capacity volume.

This matches our expectations in the degree of localized mixing effect on particle size distribution for each mixing method. Our estimates indicate that when a larger power density is supplied such as the case for ultrasonication or dispersion relative to magnetic mixing, the polydispersity of the postfiltered sample decreases. This effect is likely due to the more uniform flow field produced by the mixing method which leads to a more homogeneous and less polydisperse encapsulated particle distribution; this can also be understood based on the fact that in turbulent flows, the length scale of the smallest eddies scales with the power density as $L \sim \phi^{-1/4}$,[50] which means that turbulence develops a finer-grained eddy structure (and thus more uniform mixing state) as the power density is increased. In addition, these results are consistent with a computational fluid dynamics study comparing turbulence regimes produced by ultrasonication and agitation using a Rushton turbine in a standard tank; their results indicate that ultrasonication does indeed establish a higher and more uniform velocity distribution at a comparable power consumption to stirring.[51]

3.4. Lyophilization. Lyophilization was studied in terms of several parameters including excipient type, excipient concentration, PEG−PLA molecular weight, and reconstitution time. The results corresponding to each parameter are shown in Figures 9−11. For each trial, sizes of both filtered and unfiltered samples were measured before lyophilization and after reconstitution in aqueous solution.

Several parameters were studied with regards to lyophilization, the first being the addition of a lyophilization excipient (often known as a lyoprotectant, cryoprotectant, or lyophilization aid). Sugars and sugar alcohols are the most commonly used excipients to stabilize encapsulated NPs during lyophilization, and the specific choice of excipient depends on the system being studied.[29] The main purpose of the excipient is to prevent agglomeration of encapsulated NPs that may occur due to intermicellar fusion and coalescence during lyophilization. The two excipients that were chosen to be studied experimentally were sucrose (common table sugar) and mannitol (the reduced form of the sugar mannose). A range of polymer to lyoprotectant ratios (1:0.11−1:1.5 or 10−60% by total dry weight) has been suggested as appropriate for polymeric NPs.[29] As shown in Figure 9, postlyophilization sizes tend to decrease as a function of excipient concentration. At 0 and 10% excipient concentrations, a significant difference was not observed between sucrose and mannitol, but at 60% excipient concentration, sucrose-treated samples performed significantly better with smaller particle sizes after lyophilization in both pre- and postfiltered cases. It was therefore deemed appropriate to continue using 60% sucrose in the remaining lyophilization experiments. Although 60% sucrose was more promising as the

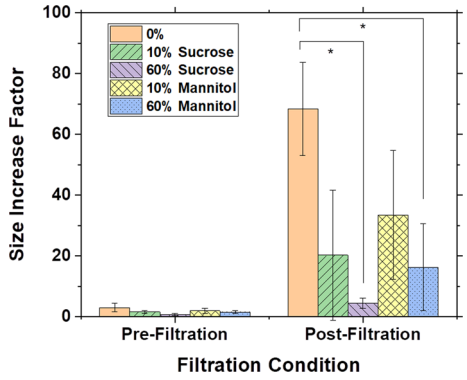

Figure 9. Size increase factor (postlyophilization diameter divided by prelyophilization diameter) based on excipient type and concentration (sucrose vs mannitol, and 0%, 10%, and 60% on total dry weight basis) for samples of PEG(5 k)-PLA(5 k)-encapsulated CWO NPs prepared with and without passing through a 0.2 μm PVDF filter. Error bars equal ±1 SD representing batch-to-batch variability. N = 4 for 0%, and remaining N = 3. Filtration was done prior to lyophilization, and reconstituted samples were not filtered.

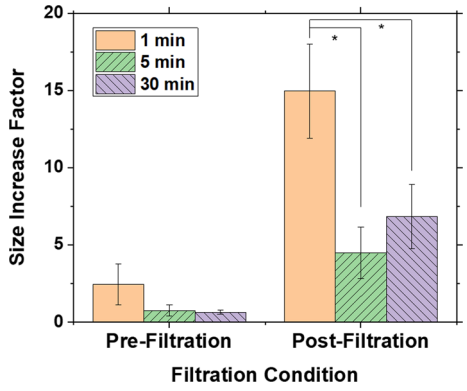

Figure 10. Size increase factor (postlyophilization diameter divided by prelyophilization diameter) based on reconstitution time (1, 5, or 30 min) for samples of PEG(5 k)-PLA(5 k)-encapsulated CWO NPs prepared with and without passing through a 0.2 μm PVDF filter. Error bars equal ±1 SD representing batch-to-batch variability. N = 3 for all trials. Filtration was done prior to lyophilization, and reconstituted samples were not filtered.

https://doi.org/10.1021/acs.iecr.0c05852
Ind. Eng. Chem. Res. 2021, 60, 7081−7096

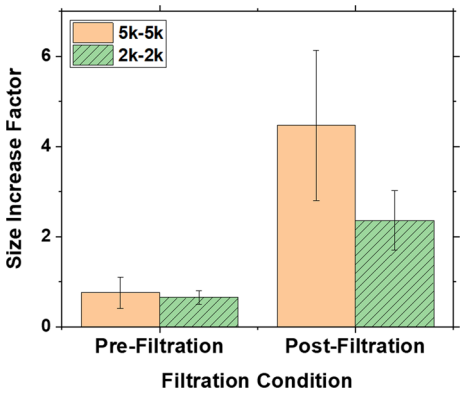

Figure 11. Size increase factor (postlyophilization diameter divided by prelyophilization diameter) based on PEG−PLA molecular weight (5 k−5 k vs 2 k−2 k) for samples of PEG−PLA encapsulated CWO NPs prepared with and without passing through a 0.2 μm PVDF filter. Error bars equal ±1 SD representing batch-to-batch variability. N = 3 for all trials. Filtration was done prior to lyophilization, and reconstituted samples were not filtered.

excipient type and concentration, there was still a significant increase in mean diameter before and after lyophilization (from 76 to 325 nm in the postfiltered case), as shown in Figure 9.

One possible explanation for these trends lies in the difference in molecular size and structure of the two excipients. Mannitol (182 Da molecular weight) is a six-carbon linear chain with six hydroxyl groups, while sucrose (342 Da molecular weight) contains two rings (glucose and fructose) connected by a glycosidic bond with eight hydroxyl groups in total. Not only is sucrose twice the size of mannitol, but it is also more rigid and thus occupies more space than mannitol. During the freeze-drying step, the excipient serves as a substitute for water,[37] and sucrose has a slightly higher propensity to the hydrogen bond with the ether oxygen of PEG in the PEG−PLA polymer chain. These structural advantages of sucrose would allow it to better interact with and shield PEG−PLA micelles from aggregating with one another. These structural advantages of sucrose would also explain the steeper trend seen for sucrose as compared to mannitol. Adding more excipient would indeed further prevent micellar agglomerates from forming by more extensively coating and stabilizing the encapsulated NPs. However, because mannitol is smaller than sucrose, it does not take up as much space as sucrose and thus would be less effective in physically shielding the PEG chains from each other. These results are consistent with previous lyophilization studies of sagopilone-loaded PEG−PLA micelles;[36] the size increase factor was smaller for sucrose compared to mannitol.

The next lyophilization parameter studied was reconstitution time. Samples lyophilized with 60% sucrose were resuspended in PBS. To determine the minimum wait time for proper dissolution and stabilization, sizes were determined at three different reconstitution times (samples kept quiescently for 1, 5, and 30 min after addition of PBS). Immediately prior to DLS size characterization, samples were vortexed. As Figure 10 demonstrates, 5 min is sufficient for proper reconstitution.

Finally, the molecular weight of PEG−PLA was studied to investigate its effect on the aggregation of product during lyophilization using 60% sucrose as the excipient. The performance of PEG(5 k)-PLA(5 k) was compared to that of PEG(2 k)-PLA(2 k) to determine whether reducing the molecular weight would be beneficial. Figure 11 shows the impact of using 2 k−2 k PEG−PLA in comparison to 5 k−5 k PEG−PLA. Though the mean hydrodynamic diameters were nearly identical regardless of polymer molecular weight, the results show that the filtered encapsulated NPs better retained small, desirable sizes after lyophilization when the 2 k−2 k polymer was used. The smaller chain length seems to have lent itself to an enhancement in the stability of the PEG−PLA self-assembly on the surfaces of CWO NPs and thus a reduction in the aggregation of encapsulated NPs during lyophilization. The 5 k−5 k and 2 k−2 k PEG−PLA materials have comparable critical micellization concentration (CMC) values in water [≈ 3.6 and 4.5 μM (measured at room temperature), respectively[52]]; this relatively small difference in CMC should not explain the qualitative gap between their lyophilization behaviors. We believe that a more reasonable explanation is as follows. Based on prior knowledge in the literature,[53] it is reasonable to expect that because of its smaller overall molecular weight, 2 k−2 k PEG−PLA prefers a micelle structure with a lower interfacial curvature than does 5 k−5 k PEG−PLA; the 2 k−2 k material forms a more stable coating on CWO NP surfaces. Further investigation is warranted in order to validate this hypothesis. It can be concluded, in the meantime, that using 2 k−2 k PEG−PLA with 60% sucrose as the excipient will significantly reduce and offset to some extent the aggregation effects associated with lyophilization.

4. CONCLUSIONS

In conclusion, CWO NPs that have been encapsulated within PEG−PLA polymeric micelles can be utilized in intratumoral administration for cancer treatment.[11,14−16] Because CWO may act as a radiosensitizer, lower doses of radiation would be needed to eradicate the tumor, therefore decreasing the probability of undesirable side effects associated with more generic forms of radiation therapy. CWO NPs are also promising as contrast agents for X-ray CT imaging. However, because CWO NPs are prone to agglomerate in aqueous physiological solutions, it is necessary to encapsulate the CWO NPs within PEG−PLA BCP micelles through solvent exchange to prevent their agglomeration and thereby achieve a favorable distribution of the NPs within the tumor. This nanoparticulate drug delivery system would reduce the toxicities and side effects that are associated with chemotherapy and radiation therapy. Several parameters (solvent type, polymer/NP ratio, mixing method, and lyophilization) were investigated in order to optimize this encapsulation procedure for future scale-up. For solvent type, we found that a less toxic solvent, acetone (Safety Class III), can be used to produce encapsulated CWO NPs with similar size characteristics compared to a more commonly used solvent for BCP-encapsulated drug/NP formulations, DMF (Safety Class II). Our study of the polymer/NP ratio shows that a higher ratio produces a smaller particle size due to faster polymer adsorption relative to NP agglomeration; we found that the ratio could be reduced from 600:1 to 50:1 without having a significant effect on size (<20% increase). Through a comparison of a few different mixing methods (ultrasonication/dispersion, ultrasonication only, dispersion only, and magnetic stirring), mixing method analysis indicates that a more homogenous and less polydisperse encapsulated particle distribution is produced by a mixing method that creates a more uniform flow field; ultrasonication/dispersion < ultrasonication only < dispersion only < magnetic stirring in postfiltration particle size PDI. Lastly, using conventional lyophilization protocols, PEG−PLA-encapsulated CWO NPs could be freeze-dried and reconstituted to produce

https://doi.org/10.1021/acs.iecr.0c05852
Ind. Eng. Chem. Res. 2021, 60, 7081−7096

reasonably sized final NP constructs. We report that using sucrose as an excipient resulted in less aggregation than mannitol at 60% or 2:3 polymer-to-lyoprotectant weight ratio and that a smaller PEG−PLA molecular weight (2 k−2 k) was found to be less prone to agglomeration than 5 k−5 k during the freeze-drying process. Further testing, including in vitro and in vivo experiments, may be conducted to study the downstream therapeutic effects of these optimized parameters that produce more monodisperse NP formulations with added lyophilization excipients.

■ ASSOCIATED CONTENT

Supporting Information

The Supporting Information is available free of charge at https://pubs.acs.org/doi/10.1021/acs.iecr.0c05852.

> Expanded tables summarizing previous literature on solvent exchange methodology and lyophilization excipient use, results of statistical tests, representative DLS histograms for pre- and postfiltered uncoated CWO NPs corresponding to Figure 5, TGA profiles for pre- and postfiltered PEG−PLA/CWO NPs used to calculate values for Table 3, and the results of the simple hydration experiment in which micelle size was determined as a function of solvent composition (PDF)

■ AUTHOR INFORMATION

Corresponding Author

You-Yeon Won − *Davidson School of Chemical Engineering and Purdue University Center for Cancer Research, Purdue University, West Lafayette, Indiana 47907, United States;* orcid.org/0000-0002-8347-6375; Email: yywon@purdue.edu

Authors

Anish P. Patel − *Davidson School of Chemical Engineering, Purdue University, West Lafayette, Indiana 47907, United States*

Christopher R. Schorr − *Davidson School of Chemical Engineering, Purdue University, West Lafayette, Indiana 47907, United States*

Dhushyanth Viswanath − *Davidson School of Chemical Engineering, Purdue University, West Lafayette, Indiana 47907, United States*

Kaustabh Sarkar − *Davidson School of Chemical Engineering, Purdue University, West Lafayette, Indiana 47907, United States*

Natalie J. Streb − *Davidson School of Chemical Engineering, Purdue University, West Lafayette, Indiana 47907, United States*

Vincenzo J. Pizzuti − *Davidson School of Chemical Engineering, Purdue University, West Lafayette, Indiana 47907, United States;* orcid.org/0000-0002-1708-3776

Rahul Misra − *Davidson School of Chemical Engineering, Purdue University, West Lafayette, Indiana 47907, United States*

Jaewon Lee − *Department of Biomedical, Biological and Chemical Engineering, University of Missouri, Columbia, Missouri 65211, United States*

Complete contact information is available at: https://pubs.acs.org/10.1021/acs.iecr.0c05852

Author Contributions

†A.P.P. and C.R.S. contributed equally to this work.

Notes

The authors declare no competing financial interest.

■ ACKNOWLEDGMENTS

Funding for this research was provided by Purdue Office of the Executive Vice President for Research and Partnerships (OEVPRP) (New NIH R01 Program), Purdue University Center for Cancer Research (PCCR, P30CA023168) (Shared Resource Biological Evaluation Project, Phase I Concept Award, and Challenge Research Award), Purdue University Discovery Park (Walther Oncology Physical Sciences & Engineering Research Embedding Program), Lodos Theranostics LLC (Gift Grant), and the School of Chemical Engineering at Purdue University. Y.Y.W. is also grateful for funding from NSF (CBET-1803968).

■ REFERENCES

(1) Tran, S.; DeGiovanni, P.-J.; Piel, B.; Rai, P. Cancer Nanomedicine: A Review of Recent Success in Drug Delivery. *Clin. Transl. Med.* **2017**, *6*, 44.

(2) Shi, J.; Kantoff, P. W.; Wooster, R.; Farokhzad, O. C. Cancer Nanomedicine: Progress, Challenges and Opportunities. *Nat. Rev. Cancer* **2017**, *17*, 20−37.

(3) Sinha, R.; Kim, G. J.; Nie, S.; Shin, D. M. Nanotechnology in Cancer Therapeutics: Bioconjugated Nanoparticles for Drug Delivery. *Mol. Cancer Ther.* **2006**, *5*, 1909−1917.

(4) Singh, R.; Lillard, J. W., Jr. Nanoparticle-Based Targeted Drug Delivery. *Exp. Mol. Pathol.* **2009**, *86*, 215−223.

(5) Tyrrell, Z. L.; Shen, Y.; Radosz, M. Fabrication of Micellar Nanoparticles for Drug Delivery through the Self-Assembly of Block Copolymers. *Prog. Polym. Sci.* **2010**, *35*, 1128−1143.

(6) Yang, D.; Yu, L.; Van, S. Clinically Relevant Anticancer Polymer Paclitaxel Therapeutics. *Cancers* **2011**, *3*, 17−42.

(7) Kawano, T.; Niidome, Y.; Mori, T.; Katayama, Y.; Niidome, T. PNIPAM Gel-Coated Gold Nanorods for Targeted Delivery Responding to a Near-Infrared Laser. *Bioconjugate Chem.* **2009**, *20*, 209−212.

(8) Pizzuti, V. J.; Viswanath, D.; Torresgrosa-Allen, S. E.; Currie, M. P.; Elzey, B. D.; Won, Y.-Y. Bilirubin-Coated Radioluminescent Particles for Radiation-Induced Photodynamic Therapy. *ACS Appl. Bio Mater.* **2020**, *3*, 4858−4872.

(9) Ishizu, K.; Hatoyama, N.; Makino, M.; Tokuno, Y.; Uchida, S. Encapsulation of Silver Nanoparticles within Micropores of Block Copolymers Constructed by Emulsion-Induced Method. *J. Polym. Sci. A Polym. Chem.* **2008**, *46*, 3429−3432.

(10) Hu, J.; Qian, Y.; Wang, X.; Liu, T.; Liu, S. Drug-Loaded and Superparamagnetic Iron Oxide Nanoparticle Surface Embedded Amphiphilic Block Copolymer Micelles for Integrated Chemotherapeutic Drug Delivery and MR Imaging. *Langmuir* **2012**, *28*, 2073−2082.

(11) Pizzuti, V. J.; Misra, R.; Lee, J.; Torregrosa-Allen, S. E.; Currie, M. P.; Clark, S. R.; Patel, A. P.; Schorr, C. R.; Jones-Hall, Y.; Childress, M. O.; Plantenga, J. M.; Rancilio, N. J.; Elzey, B. D.; Won, Y.-Y. Folic Acid-Conjugated Radioluminescent Calcium Tungstate Nanoparticles as Radio-Sensitizers for Cancer Radiotherapy. *ACS Biomater. Sci. Eng.* **2019**, *5*, 4776−4789.

(12) Saad, W. S.; Prud'homme, R. K. Principles of Nanoparticle Formation by Flash Nanoprecipitation. *Nano Today* **2016**, *11*, 212−227.

(13) *ICH Quality Guidelines: An Implementation Guide* | *Wiley* https://www.wiley.com/en-us/ICH+Quality+Guidelines%3A+An+Implementation+Guide-p-9781118971116 (accessed May 11, 2020).

(14) Lee, J.; Rancilio, N. J.; Poulson, J. M.; Won, Y.-Y. Block Copolymer-Encapsulated $CaWO_4$ Nanoparticles: Synthesis, Formula-

tion, and Characterization. *ACS Appl. Mater. Interfaces* **2016**, *8*, 8608−8619.
(15) Jo, S. D.; Lee, J.; Joo, M. K.; Pizzuti, V. J.; Sherck, N. J.; Choi, S.; Lee, B. S.; Yeom, S. H.; Kim, S. Y.; Kim, S. H.; Kwon, I. C.; Won, Y.-Y. PEG−PLA-Coated and Uncoated Radio-Luminescent $CaWO_4$ Micro- and Nanoparticles for Concomitant Radiation and UV-A/Radio-Enhancement Cancer Treatments. *ACS Biomater. Sci. Eng.* **2018**, *4*, 1445−1462.
(16) Misra, R.; Sarkar, K.; Lee, J.; Pizzuti, V. J.; Lee, D. S.; Currie, M. P.; Torregrosa-Allen, S. E.; Long, D. E.; Durm, G. A.; Langer, M. P.; Elzey, B. D.; Won, Y.-Y. Radioluminescent Nanoparticles for Radiation-Controlled Release of Drugs. *J. Controlled Release* **2019**, *303*, 237−252.
(17) Lee, J.; Choi, S.; Kim, K. H.; Heng, H. G.; Torregrosa-Allen, S. E.; Ramsey, B. S.; Elzey, B. D.; Won, Y.-Y. Nontoxic Formulations of Scintillation Nanocrystals for Use as X-Ray Computed Tomography Contrast Agents. *Bioconjugate Chem.* **2017**, *28*, 171−182.
(18) Kim, D. H.; Wei, A.; Won, Y.-Y. Preparation of Super-Stable Gold Nanorods via Encapsulation into Block Copolymer Micelles. *ACS Appl. Mater. Interfaces* **2012**, *4*, 1872−1877.
(19) Song, J.; Yang, X.; Jacobson, O.; Huang, P.; Sun, X.; Lin, L.; Yan, X.; Niu, G.; Ma, Q.; Chen, X. Ultrasmall Gold Nanorod Vesicles with Enhanced Tumor Accumulation and Fast Excretion from the Body for Cancer Therapy. *Adv. Mater.* **2015**, *27*, 4910−4917.
(20) Kannaiyan, S.; Narayanan, T. G. A.; Sarathy, P. K.; Sudhakar, N.; Krishnan, R. Synthesis and Kinetic Studies on Controlled Release of 6-Thioguanine Entrapped Polyethene Glycol-Co-Polylactic Acid Polymer Nanoparticles. *Int. J. Chem. React. Eng.* **2011**, *9*, No. A101.
(21) Frounchi, M.; Shamshiri, S. Magnetic Nanoparticles-loaded PLA/PEG Microspheres as Drug Carriers. *J. Biomed. Mater. Res. A* **2015**, *103*, 1893−1898.
(22) Wei, Q.; Li, T.; Wang, G.; Li, H.; Qian, Z.; Yang, M. Fe3O4 Nanoparticles-Loaded PEG−PLA Polymeric Vesicles as Labels for Ultrasensitive Immunosensors. *Biomaterials* **2010**, *31*, 7332−7339.
(23) Zhang, Q.; Zhu, J.; Song, L.; Zhang, J.; Kong, D.; Zhao, Y.; Wang, Z. Engineering Magnetic-Molecular Sequential Targeting Nanoparticles for Anti-Cancer Therapy. *J. Mater. Chem. B* **2013**, *1*, 6402.
(24) Gao, X.; Luo, W. Prostate Stem Cell Antigen-Targeted Nanoparticles with Dual Functional Properties: In Vivo Imaging and Cancer Chemotherapy. *Int. J. Nanomed.* **2012**, 4037.
(25) Li, K.; Ding, D.; Huo, D.; Pu, K.-Y.; Thao, N. N. P.; Hu, Y.; Li, Z.; Liu, B. Conjugated Polymer Based Nanoparticles as Dual-Modal Probes for Targeted In Vivo Fluorescence and Magnetic Resonance Imaging. *Adv. Funct. Mater.* **2012**, *22*, 3107−3115.
(26) Liu, P.; Li, J.; Zhang, C.; Xu, L. X. Micro-CT Molecular Imaging of Tumor Angiogenesis Using a Magnetite Nano-Cluster Probe. *J. Biomed. Nanotechnol.* **2013**, *9*, 1041−1049.
(27) Ai, H.; Flask, C.; Weinberg, B.; Shuai, X.-T.; Pagel, M. D.; Farrell, D.; Duerk, J.; Gao, J. Magnetite-Loaded Polymeric Micelles as Ultrasensitive Magnetic-Resonance Probes. *Adv. Mater.* **2005**, *17*, 1949−1952.
(28) Marrache, S.; Choi, J. H.; Tundup, S.; Zaver, D.; Harn, D. A.; Dhar, S. Immune Stimulating Photoactive Hybrid Nanoparticles for Metastatic Breast Cancer. *Integr. Biol.* **2013**, *5*, 215−223.
(29) Lee, S. W.; Kim, G. H.; Seo, M. H. Polymer Nanoparticle Freeze-Dried Product, and Preparation Method Therefor. US20180000946A1, January 4 , 2018.
(30) Abdelwahed, W.; Degobert, G.; Fessi, H. A Pilot Study of Freeze Drying of Poly(Epsilon-Caprolactone) Nanocapsules Stabilized by Poly(Vinyl Alcohol): Formulation and Process Optimization. *Int. J. Pharm.* **2006**, *309*, 178−188.
(31) Bozdag, S.; Dillen, K.; Vandervoort, J.; Ludwig, A. The Effect of Freeze-Drying with Different Cryoprotectants and Gamma-Irradiation Sterilization on the Characteristics of Ciprofloxacin HCl-Loaded Poly(D,L-Lactide-Glycolide) Nanoparticles. *J. Pharm. Pharmacol.* **2005**, *57*, 699−707.
(32) Sameti, M.; Bohr, G.; Ravi Kumar, M. N. V.; Kneuer, C.; Bakowsky, U.; Nacken, M.; Schmidt, H.; Lehr, C.-M. Stabilisation by Freeze-Drying of Cationically Modified Silica Nanoparticles for Gene Delivery. *Int. J. Pharm.* **2003**, *266*, 51−60.
(33) Tian, J.; Yan, C.; Liu, K.; Tao, J.; Guo, Z.; Liu, J.; Zhang, Y.; Xiong, F.; Gu, N. Paclitaxel-Loaded Magnetic Nanoparticles: Synthesis, Characterization, and Application in Targeting. *J. Pharm. Sci.* **2017**, *106*, 2115−2122.
(34) Zambaux, M. F.; Bonneaux, F.; Gref, R.; Dellacherie, E.; Vigneron, C. MPEO-PLA Nanoparticles: Effect of MPEO Content on Some of Their Surface Properties. *J. Biomed. Mater. Res.* **1999**, *44*, 109−115.
(35) Miller, T.; van Colen, G.; Sander, B.; Golas, M. M.; Uezguen, S.; Weigandt, M.; Goepferich, A. Drug Loading of Polymeric Micelles. *Pharm. Res.* **2013**, *30*, 584−595.
(36) Richter, A.; Olbrich, C.; Krause, M.; Hoffmann, J.; Kissel, T. Polymeric Micelles for Parenteral Delivery of Sagopilone: Physicochemical Characterization, Novel Formulation Approaches and Their Toxicity Assessment in Vitro as Well as in Vivo. *Eur. J. Pharm. Biopharm.* **2010**, *75*, 80−89.
(37) de Jaeghere, F.; Allémann, E.; Feijen, J.; Kissel, T.; Doelker, E.; Gurny, R. Freeze-Drying and Lyopreservation of Diblock and Triblock Poly(Lactic Acid)−Poly(Ethylene Oxide) (PLA−PEO) Copolymer Nanoparticles. *Pharm. Dev. Technol.* **2000**, *5*, 473−483.
(38) *CRC handbook of chemistry and physics [2019−2020] : a ready-reference book of chemical and physical data (Book, 2019)* [WorldCat.org] https://www.worldcat.org/title/crc-handbook-of-chemistry-and-physics-2019-2020-a-ready-reference-book-of-chemical-and-physical-data/oclc/1114281745?referer=di&ht=edition (accessed May 11, 2020).
(39) Nagarajan, R. "Frozen" Micelles: Polymer Nanoparticles of Controlled Size by Self-Assembly. In *Nanoparticles: Synthesis, Stabilization, Passivation, and Functionalization*; ACS Symposium Series; American Chemical Society, 2008; *996*, 341−356. DOI: 10.1021/bk-2008-0996.ch024.
(40) Thorp, J. S.; Ammar, E. A. E. The Dielectric Constants of CaWO4, Nd/CaWO4 and Gd/CaWO4. *J. Mater. Sci.* **1975**, *10*, 918−922.
(41) Israelachvili, J. N. *Intermolecular and Surface Forces*, Third edition.; Elsevier, Academic Press: Amsterdam, 2011.
(42) Cleasby, J. L. Is Velocity Gradient a Valid Turbulent Flocculation Parameter? *J. Environ. Eng.* **1984**, *110*, 875−897.
(43) Holland, F. A.; Bragg, R. *Fluid Flow for Chemical Engineers*; Edward Arnold: London, 1995.
(44) Won, Y.-Y.; Meeker, S. P.; Trappe, V.; Weitz, D. A.; Diggs, N. Z.; Emert, J. I. Effect of Temperature on Carbon-Black Agglomeration in Hydrocarbon Liquid with Adsorbed Dispersant. *Langmuir* **2005**, *21*, 924−932.
(45) Dotson, N. A. *Polymerization Process Modeling*; Wiley-VCH: New York, 1996.
(46) Lin, M. Y.; Lindsay, H. M.; Weitz, D. A.; Ball, R. C.; Klein, R.; Meakin, P. Universal Reaction-Limited Colloid Aggregation. *Phys. Rev. A* **1990**, *41*, 2005−2020.
(47) Evans, D. F.; Wennerström, H. The Colloidal Domain: Where Physics, Chemistry, Biology, and Technology Meet, 2nd ed.; *Advances in interfacial engineering series*; Wiley-VCH: New York, 1999.
(48) Seinfeld, J. H.; Pandis, S. N. *Atmospheric Chemistry and Physics: From Air Pollution to Climate Change*, Third edition.; John Wiley & Sons: Hoboken, New Jersey, 2016.
(49) Weetman, R. J. Development of Transitional Flow Mixing Impeller. In *Fluid Mechanics of Mixing: Modelling, Operations and Experimental Techniques*; King, R., Ed.; Fluid Mechanics and Its Applications ; Springer Netherlands: Dordrecht, 1992; 19−26. DOI: 10.1007/978-94-015-7973-5_3.
(50) Deen, W. M. *Analysis of Transport Phenomena; Topics in chemical engineering*; Oxford University Press: New York, 1998.
(51) Parvizian, F.; Rahimi, M.; Faryadi, M.; Abdulaziz Alsairafi, A. Comparison between Mixing in Novel High Frequency Sonoreactor and Stirred Tank Reactor. *Eng. Appl. Comput. Fluid Mech.* **2012**, *6*, 295−306.
(52) Garofalo, C.; Capuano, G.; Sottile, R.; Tallerico, R.; Adami, R.; Reverchon, E.; Carbone, E.; Izzo, L.; Pappalardo, D. Different Insight into Amphiphilic PEG-PLA Copolymers: Influence of Macromolecular

Architecture on the Micelle Formation and Cellular Uptake. *Biomacromolecules* **2014**, *15*, 403−415.
(53) Won, Y. Y.; Bates, F. S. Nonionic Block Copolymer Wormlike Micelles. *Giant Micelles Prop. Appl.* **2007**, 417−452.

https://doi.org/10.1021/acs.iecr.0c05852
Ind. Eng. Chem. Res. 2021, 60, 7081−7096